Letter

Dynamical Hubbard approach to correlated materials: The case of transition-metal monoxides

Mario Caserta [1,*,†] Tommaso Chiarotti [2,†] Marco Vanzini [3] and Nicola Marzari [1,4,5]

[1]*Theory and Simulation of Materials (THEOS), and National Centre for Computational Design and Discovery of Novel Materials (MARVEL), École Polytechnique Fédérale de Lausanne, CH-1015 Lausanne, Switzerland*

[2]*Department of Applied Physics and Materials Science, California Institute of Technology, Pasadena, California 91125, USA*

[3]*Collège Champittet, Pully, Switzerland*

[4]*Theory of Condensed Matter, Cavendish Laboratory, University of Cambridge, Cambridge CB3 0US, United Kingdom*

[5]*PSI Center for Scientific Computing, Theory and Data, 5232 Villigen PSI, Switzerland*

(Received 12 March 2025; accepted 4 August 2026; published 19 August 2026)

Electronic correlations beyond static mean-field theories are of fundamental importance in describing the properties of complex materials—such as transition-metal oxides—where the low-energy physics is driven by localized d or f electrons. Here, we show that it is possible to capture these correlations with a local and dynamical self-energy, extending to the spin-polarized and multisite case in our recently introduced dynamical Hubbard functional formulation. We apply this formalism to the prototypical transition-metal monoxide series of MnO, FeO, CoO, and NiO in their ground state, finding excellent agreement with experiments for the spectral properties. The results are comparable or improved with respect to state-of-the-art theories, both for the densities of states and for the spectral functions—including band renormalization and spectral weight transfer—in a numerically efficient and physically insightful treatment of correlations amenable to the study of realistic, complex materials.

DOI: 10.1103/y7gb-q22g

Binary transition-metal oxides MnO, FeO, CoO, and NiO are some of the most studied and characterized materials, both experimentally [1–6] and theoretically [7–12]. These compounds have been categorized, respectively, as Mott and charge-transfer insulators, within the common Zaanen-Sawatzky-Allen scheme [13], and they are insulating both above and below their Néel temperatures. They represent ideal test cases for electronic structure methods thanks to both their simple crystal structures [rocksalt ($Fm3m$) in the paramagnetic phase and slightly distorted rhombohedral ($R3m$) with two transition-metal (TM) ions per unit cell in the low-temperature AFM-II phase], and for displaying gradually varying properties throughout the filling of the $3d$ shell. Describing quantitatively the complex interplay between the electronic localization on the TM sites and the hybridization with the ligands is a challenging task for Kohn-Sham density-functional theory (DFT) with standard semilocal functionals [5,9,14], as it underestimates the electronic gap in MnO and NiO, and fails to predict the insulating state of CoO and FeO. These shortcomings are inherited by many-body perturbation theory approaches, such as G_0W_0 and GW_0, when they start from the DFT metallic electronic structure [9,15]. Improvements in the description of the excitation spectrum can be obtained using, e.g., DFT + U and hybrid functionals [9,12,14,16], where the insulating states and gap magnitudes are recovered, gauged by the effective U and exchange-fraction parameters. These are often fitted to reproduce experimental data, thus hindering the predictive first-principles nature of the methods, or are unable to systematically reproduce the full spectral properties across the series [9,12,16]. To improve on G_0W_0 and GW_0 results, one can instead either start from DFT + U [17,18] or hybrid ground states [19], and/or introduce vertex corrections in quasiparticle self-consistent extensions (QSG$\hat{\text{W}}$) [10,20]. While this improves the description of gap magnitudes and hybridization effects typical of charge-transfer insulators, the ability to describe k-resolved spectral weight transfer and band renormalization, prototypical features of electronic correlations [21,22], requires a theoretical framework that incorporates complex and frequency-dependent self-energies, giving access to correlation-induced particle lifetimes [8,9]. DFT + U and hybrids are inherently static mean-field solutions, while in full GW or QSGW and QSG$\hat{\text{W}}$ the full frequency dependence is commonly discarded because of the heavy computational cost and numerical complexity. Given that dynamical frameworks allow for energetic corrections and localization pathways inaccessible to static solutions, DFT + DMFT [23,24] has become the theoretical tool to model complex transition-metal oxides [9,25]. In dynamical mean-field theory (DMFT), the local correlated subspace, often the TM d or f shell, is mapped onto an effective

*Contact author: mario.caserta@epfl.ch

†These authors contributed equally to this work.

Anderson impurity model [26], which can be solved exactly, often with Monte Carlo methods [27], and embedded back into the DFT solution in a self-consistent cycle. Thus, DFT + DMFT allows to describe local dynamical electronic correlations and fluctuating magnetic moments, improving the description of electronic gaps, band renormalization, and spectral weight transfer. However, it also leads to high computational costs and increased numerical complexity, with exact solutions scaling exponentially with system size [27,28]. Similarly to DFT + DMFT, other approaches that include high-order correlation effects and require exact impurity solutions are GW + self-energy embedding theory (GW + SEET) [29] for MnO and NiO, and GW + DMFT [30] for NiO.

In this Letter, we show that a simple and transparent dynamical formulation, obtained from the generalization of DFT + U to host a local frequency-dependent screened interaction, is able to capture all the correlated-electron signatures of gap opening, band renormalization, and spectral weight transfer, in excellent agreement with experimental photoemission spectroscopy (PES) and inverse photoemission spectroscopy (IPES) data [2,5,6,31] and state-of-the-art DFT + DMFT results [8,9], in all four compounds. This is achieved by solving the Dyson equation with the algorithmic-inversion method on sum over poles (AIM-SOP) for a dynamical Hubbard functional (dynH) [32], generalized here to treat magnetic systems with multiple TM sites. The functional derivative of the dynH functional with respect to the local Green's function provides the dynH self-energy localized on the correlated manifold. We apply here the framework to study the MnO, FeO, CoO, and NiO series, obtaining beyond state-of-the-art results for the spectral properties of these materials. In all cases, a very good agreement with experiments is found, including the small gap for FeO, in agreement with the experimental results [3] and in contrast with DFT + DMFT [8] and QSG$\hat{\text{W}}$ [10] that predict a wide gap for all four monoxides. Moreover, it is shown that in the case of NiO the present approach predicts electronic bands present in the experimental angle-resolved photoemission spectroscopy (ARPES) data [5,6] that disappear in the strong correlation regime of the DMFT impurity solution [7,8].

The dynamical Hubbard functional [32] has been introduced to address local dynamical correlations, giving accurate results for the spectral properties of prototypical correlated oxide $SrVO_3$, in agreement with experimental data [33] and state-of-the-art GW + extendend dynamical mean-field theory (GW + EDMFT) calculations [22,34]. Here, we generalize the functional to the multisite collinear spin-polarized case, in order to treat magnetic systems. The generalization of Eq. (8) in Ref. [32] to spin-dependent cases involves the spin polarization of the momentum-band Green's function and of the random-phase approximation (RPA) screened interaction. From the convolution of the two, one arrives at a local spin-dependent exchange and correlation self-energy of the form [35]

$$\begin{aligned}\boldsymbol{\Sigma}^{\sigma,I}_{\text{dynH}}(\omega) &= 2\pi i \frac{\partial \Phi_{\text{dynH}}\left[\mathbf{G}^{\sigma}_{I}\right]}{\partial \mathbf{G}^{\sigma}_{I}} \\ &= -\int d\omega' U_I(\omega')\mathbf{G}^{\sigma}_{I}(\omega+\omega') + \frac{U^{\infty}_{I}}{2}. \end{aligned} \quad (1)$$

The local spin Green's function is defined as $\mathbf{G} = P^{\dagger}GP$, where the projectors P transform from the momentum-band $(\mathbf{k}, n)$ indexes to the (m) index, representing the magnetic quantum number of an atomiclike orbitals ϕ_m (e.g., $3d$ shell with $l = 2$ and $m = -2, -1, 0, 1, 2$) centered on each transition-metal site I in the cell. $U(\omega)$ is the local average of the direct matrix elements in the basis of the N_d atomiclike orbitals [36] of the screened Coulomb interaction [37]

$$U_I(\omega) = \frac{1}{2N_d}\sum_{m\sigma}\left\langle \phi^{\sigma}_{m,I}\phi^{\sigma}_{m,I}\middle| W_{\text{RPA}}(\mathbf{r},\mathbf{r}',\omega)\middle|\phi^{\sigma}_{m,I}\phi^{\sigma}_{m,I}\right\rangle, \quad (2)$$

calculated from the RPA spin-DFT polarization function, and U^{∞} is its fully unscreened value (local matrix element of bare Coulomb potential). The expression in Eq. (1) can be seen as a complex and frequency-dependent generalization of the Dudarev rotationally invariant formulation of DFT + U potential [39], now hosting a dynamical and complex time-ordered effective interaction potential, plus a static double-counting term [32,40]. It also extends the model self-energy derived by Vanzini and Marzari [40] to a full functional formulation. It is important to stress that the local dynamical interaction used here is screened by all, local and nonlocal, processes at the RPA level. The local self-energy of Eq. (1) is then upfolded to the k space, using $\Sigma = P\boldsymbol{\Sigma}_{\text{dynH}}P^{\dagger}$. The k-resolved spectral function and density of states are then obtained from the Green's function that solves the Dyson equation $G^{-1} = G_0^{-1} - \Sigma$. The solution of the Dyson equation is achieved via the aforementioned AIM-SOP [32,41], where both the local screened Coulomb interaction and local Green's function are represented as sums over first-order poles and amplitudes. Importantly, when looking at spectral properties, AIM-SOP avoids the use of imaginary Matsubara frequencies as in the most common impurity solutions used in DMFT [27], which requires the analytic continuation to the real axis, thus hindering the accuracy of the calculations [42]. We refer to the Supplemental Material [43] for the SOP representations of the local dynamical screened $U(\omega)$ and to Ref. [32] for the overall AIM-SOP framework. Importantly, we find that the full solution of the Dyson equation for these materials is crucial when looking at k-resolved spectral functions, where the description of band crossings has to be properly accounted for. Please note that, if a SOP representation for the self-energy is adopted (as it is done in this work), the cost of the dynamical Hubbard self-energy in Eq. (1) is $N_p^G N_p^U N_k (N_M)^2$, with N_p^G the number of poles of the Green's function, U_p the poles of $U(\omega)$, N_k the number of k points, and N_M the number of orbitals in the local manifold. This scaling has to be compared to the exponential scaling of DMFT-like methods, though with possible reductions when approximations are made [28]. For the DFT ground-state calculation, we use the regularized-restored Strongly Constrained and Appropriately Normed (r2SCAN) functional [44], owing to its correct prediction of an insulating phase in all four compounds [11] on an equal footing [45]. Computational details, DFT band structures, DFT + dynH projected density of states can be found in the Supplemental Material [43].

In Fig. 1, we show the total density of states of one-shot DFT + dynH for the AFM phase of the four monoxides, together with state-of-the-art charge self-consistent

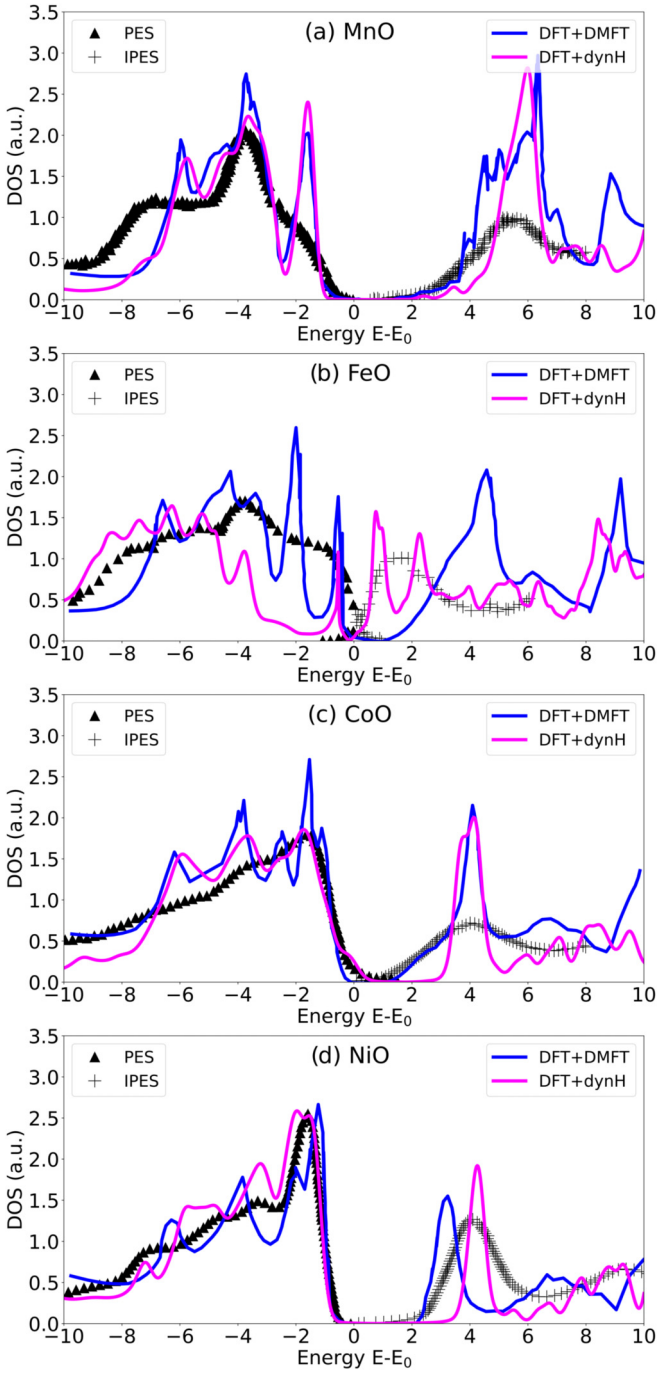

FIG. 1. Density of states for one-shot DFT + dynH (solid magenta lines) for MnO [panel (a)], FeO [panel (b)], CoO [panel (c)], and NiO [panel (d)], compared to DFT + DMFT [8] (solid blue lines). Experimental data in black markers from Ref. [2] for MnO, Ref. [3] for FeO, Ref. [31] for CoO, and Ref. [38] for NiO. A broadening of 0.1 eV has been used.

DFT + eDMFT [8] and PES/IPES experiments [1–3,31]. For MnO, Fig. 1(a), the occupied density of states (DOS) is consistent with DFT + DMFT results [8], where the overall bandwidth is slightly contracted with respect to the experimental one [2], as the high-energy satellites above remain elusive to both DFT + DMFT [8] and DFT + dynH (and also in QSGŴ calculations [10]). The lowest unoccupied molecular orbital (LUMO) excitation at 5 eV above Fermi appears to be in agreement with IPES data in position, width, and intensity. For FeO [Fig. 1(b)], DFT + dynH predicts a small gap of about 2 eV, in agreement with the IPES data in Ref. [3] and in contrast with state-of-the-art DFT + DMFT [9] and QSGŴ [10], which predict wide gaps for all four monoxides. The decrease in intensity after the first excitations is also well described by DFT + dynH. It can be seen that the main difference between DFT + dynH and DFT + DMFT results in the occupied part is the larger distance between the a_{1g} highest occupied molecular orbital (HOMO) excitation and the rest of the occupied spectrum. The O($2p$)/Fe($3d$) peak of e_g symmetry in fact appears around −4 eV, in contrast with the −2.4 eV of DFT + DMFT, as it can also be seen in the k-resolved spectral functions [panel (b) of Fig. 3 and Fig. 1 of Ref. [8]]. The dip between the first and second ionization peaks (appearing also in QSGŴ [10]) cannot be seen in the PES spectrum, though the total valence bandwidths of approximately 10 eV in DFT + dynH match quite well. For CoO, in Fig. 1(c), the DOS compares well with both DFT + DMFT and PES data. The main difference with the former resides in the first addition peaks, since in DFT + dynH the two empty states of t_g and e_g symmetry have comparable weight, whereas in DFT + DMFT the weight is mainly transferred to the higher-energy one, resulting in a single peak and a minor bump at 2.4 eV. The main peak at 3.5 eV is slightly lower than the DFT + DMFT one at 4 eV. For NiO [Fig. 1(d)], it can be seen that the agreement between the main experimental peaks [38], in both addition and removal excitations, is very good, especially for the main addition peak at 4 eV and the sharp increase in the occupied spectrum. In Fig. 2, NiO ARPES data and k-resolved spectral functions along the ΓX direction are shown, where all data from normal [4,6] and off-normal

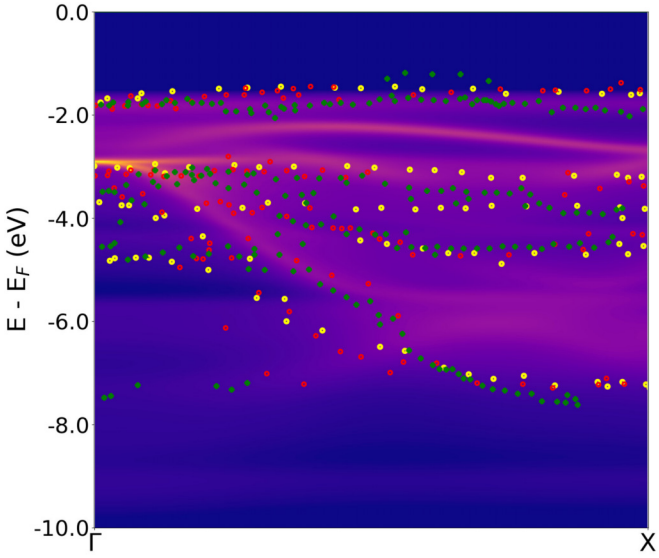

FIG. 2. DFT + dynH spectral function (purple/blue colormap) and experimental ARPES data for NiO (AFM). The red (normal) and yellow (off-normal) dots represent emission data from Ref. [5]. Green square data are normal emission from Ref. [6]. Experimental data have been aligned at the top of the valence band in the Γ point, it being the most accurate in resolution [5]. A broadening of 0.015 eV has been used.

[5] emission are collected. The overall DFT + dynH bandwidth of 6 eV is consistent with the ARPES data. The flat Ni($3d$)/O($2p$) bands at the top, associated with the Zhang-Rice doublet bound state [46,47], can be recognized, as well as the flat Ni($3d$)/O($2p$) bands around −3 eV. The two dispersing O($2p$) bands departing from Γ and extending at around −4.4 and −8 eV are also present. As it can be seen from the projected DOS (see also Fig. 8 in the Supplemental Material [43]), the actual character of the valence band excitations is mixed, confirming the charge-transfer nature of the compound, as the first addition peak is mainly of Ni e_g character. The most relevant difference between the DFT + dynH and DFT + DMFT results [7,8] is the presence of the dispersing band at −8 eV and the AFM flat band at around −4 eV, both close to Γ. They can be labeled as AFM bands as they are missing in nonmagnetic DFT calculations, while they appear in the spin-DFT broken symmetry AFM solution [5]. Their vanishing spectral weight in the DFT + DMFT spectrum and absence in the ARPES data of Ref. [4] were conjectured [8,9] to be a signature of strong correlations. It is important to note, then, that these states are present both in ARPES data [5,6] and in our DFT + dynH results. In fact, in the present work the effective screened interaction is calculated at the first order in perturbation theory, with a zero-frequency limit of $U(0) = 5.3$ eV, which is half of the effective U value used in the DFT + DMFT calculations [8,9]. The slight underestimation of the AFM bands around −4 eV could be a feature of the r2SCAN starting point, a lack of self-consistency, or the intrinsically approximate nature of the double-counting term. It is important to note that, when comparing theoretical spectral functions and experimental ARPES points, the lack of signal in the latter can be due to the (vanishing) matrix elements of the dipole operator. Moreover, in the region between −1 and −3 eV in Fig. 4 (or Fig. 13) in Ref. [5], other transitions are present, defined as subcomponents of the main feature A (see Fig. 11 for their blown-up view). See page 44 in Ref. [5] for further analysis on those components.

We show in Fig. 3 the k-resolved spectral functions for all four monoxides on a standard path. In agreement with DFT + DMFT [8], it can be seen that MnO possesses the sharpest bands, whereas a stronger spectral weight transfer from the quasi-particle (QP) peaks to the satellites appears in FeO, CoO, and NiO [48]. We stress the impressive similarity with the spectral functions presented in Ref. [8], which are obtained with an (expensive) nonperturbative solution of an effective impurity model.

In conclusion, in this work we have (1) generalized the dynamical Hubbard functional of Ref. [32] to the treatment of magnetic systems and (2) applied the framework to study valence and conduction spectral functions of the prototypical Mott-Hubbard/charge-transfer monoxide series of MnO, FeO, CoO, and NiO. We obtain remarkable agreement with PES/IPES and ARPES experimental data and state-of-the-art DFT + DMFT calculations [8,9], in a transparent and inexpensive formulation. The fundamental gaps and relative intensities and overall bandwidth of valence and conduction excitations appear to be consistent with experimental data

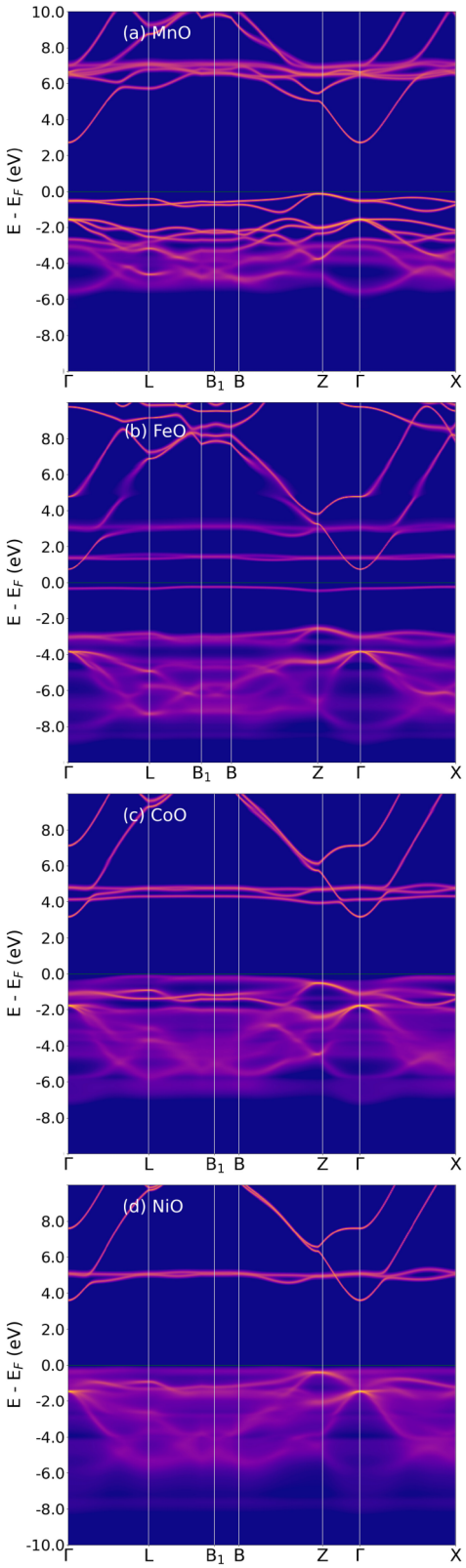

FIG. 3. DFT + dynH k-resolved spectral functions (colormap) for MnO [panel (a)], FeO [panel (b)], CoO [panel (c)], and NiO [panel (d)]. The zero of the energy is set at the top of the valence band. A broadening of 0.015 eV has been used.

for all four monoxides. Moreover, the general features of the spectral function for NiO along the Γ-X direction are in close agreement with available experimental data [5,6]. The dispersing bottom of the valence band and the characteristic flat antiferromagnetic bands are found, at variance with previous calculations [7,8], where these bands show an almost completely vanishing spectral weight.

Importantly, the present dynamical framework provides access to particle lifetimes, satellites, spectral-weight transfer, and band renormalization, i.e., fundamental signatures of electron correlations, unavailable to static methods such as hybrid functionals and DFT + U, or to QSG$\hat{\mathrm{W}}$. In particular, DFT + dynH, with appealing simplicity, minimal computational cost, and without free parameters, proves to be an efficient tool for predicting electronic structure properties of complex oxides with various degrees of symmetry-broken orbital orderings and hybridizations, thus posing itself as a promising tool for simulating realistic correlated materials, which may be prohibitive for methods employing exact solutions. Furthermore, the somewhat improved scaling of the method opens the possibility to address the computation of correlated solids with f or higher orbitals, e.g., lanthanides, that remain difficult to address (as they are computationally costly) with other state-of-the-art (nonperturbative) frameworks.

M.C. was supported with funds from Bosch-Forschungsstiftung im Stifterverband. We also acknowledge the support of the Swiss National Science Foundation (SNSF) through Grant No. 2000200-213082 and the NCCR MARVEL, a National Centre of Competence in Research, Grant No. 205602. The authors wish to thank Lucia Reining, Max Amsler, Georgy Samsonidze, and Thomas Eckl for the many fruitful discussions.

Data availability. The data that support the findings of this article are not publicly available upon publication because it is not technically feasible and/or the cost of preparing, depositing, and hosting the data would be prohibitive within the terms of this research project. The data are available from the authors upon reasonable request.

[1] G. A. Sawatzky and J. W. Allen, Magnitude and origin of the band gap in NiO, Phys. Rev. Lett. **53**, 2339 (1984).

[2] J. van Elp, R. H. Potze, H. Eskes, R. Berger, and G. A. Sawatzky, Electronic structure of MnO, Phys. Rev. B **44**, 1530 (1991).

[3] R. Zimmermann, P. Steiner, R. Claessen, F. Reinert, S. Hüfner, P. Blaha, and P. Dufek, Electronic structure of 3d-transition-metal oxides: On-site Coulomb repulsion versus covalency, J. Phys.: Condens. Matter **11**, 1657 (1999).

[4] Z.-X. Shen, J. W. Allen, P. A. P. Lindberg, D. S. Dessau, B. O. Wells, A. Borg, W. Ellis, J. S. Kang, S.-J. Oh, I. Lindau, and W. E. Spicer, Photoemission study of CoO, Phys. Rev. B **42**, 1817 (1990).

[5] Z.-X. Shen, R. S. List, D. S. Dessau, B. O. Wells, O. Jepsen, A. J. Arko, R. Barttlet, C. K. Shih, F. Parmigiani, J. C. Huang, and P. A. P. Lindberg, Electronic structure of NiO: Correlation and band effects, Phys. Rev. B **44**, 3604 (1991).

[6] H. Kuhlenbeck, G. Odörfer, R. Jaeger, G. Illing, M. Menges, T. Mull, H.-J. Freund, M. Pöhlchen, V. Staemmler, S. Witzel, C. Scharfschwerdt, K. Wennemann, T. Liedtke, and M. Neumann, Molecular adsorption on oxide surfaces: Electronic structure and orientation of NO on NiO(100)/Ni(100) and on NiO(100) as determined from electron spectroscopies and *ab initio* cluster calculations, Phys. Rev. B **43**, 1969 (1991).

[7] J. Kuneš, V. I. Anisimov, S. L. Skornyakov, A. V. Lukoyanov, and D. Vollhardt, NiO: Correlated band structure of a charge-transfer insulator, Phys. Rev. Lett. **99**, 156404 (2007).

[8] S. Mandal, K. Haule, K. M. Rabe, and D. Vanderbilt, Influence of magnetic ordering on the spectral properties of binary transition metal oxides, Phys. Rev. B **100**, 245109 (2019).

[9] S. Mandal, K. Haule, K. M. Rabe, and D. Vanderbilt, Systematic beyond-DFT study of binary transition metal oxides, npj Comput. Mater. **5**, 115 (2019).

[10] M. S. Abdallah and A. Pasquarello, Quasiparticle self-consistent *GW* with effective vertex corrections in the polarizability and the self-energy applied to MnO, FeO, CoO, and NiO, Phys. Rev. B **110**, 155105 (2024).

[11] Y. Zhang, J. Furness, R. Zhang, Z. Wang, A. Zunger, and J. Sun, Symmetry-breaking polymorphous descriptions for correlated materials without interelectronic U, Phys. Rev. B **102**, 045112 (2020).

[12] M. Cococcioni and S. de Gironcoli, Linear response approach to the calculation of the effective interaction parameters in the LDA + U method, Phys. Rev. B **71**, 035105 (2005).

[13] J. Zaanen, G. A. Sawatzky, and J. W. Allen, Band gaps and electronic structure of transition-metal compounds, Phys. Rev. Lett. **55**, 418 (1985).

[14] V. I. Anisimov, J. Zaanen, and O. K. Andersen, Band theory and Mott insulators: Hubbard U instead of Stoner I, Phys. Rev. B **44**, 943 (1991).

[15] F. Aryasetiawan and O. Gunnarsson, Electronic structure of NiO in the *GW* approximation, Phys. Rev. Lett. **74**, 3221 (1995).

[16] V. I. Anisimov, F. Aryasetiawan, and A. I. Lichtenstein, First-principles calculations of the electronic structure and spectra of strongly correlated systems: The LDA + U method, J. Phys.: Condens. Matter **9**, 767 (1997).

[17] H. Jiang, R. I. Gomez-Abal, P. Rinke, and M. Scheffler, First-principles modeling of localized d states with the *GW* @LDA + U approach, Phys. Rev. B **82**, 045108 (2010).

[18] S. Das, J. E. Coulter, and E. Manousakis, Convergence of quasiparticle self-consistent *GW* calculations of transition-metal monoxides, Phys. Rev. B **91**, 115105 (2015).

[19] C. Rödl, F. Fuchs, J. Furthmüller, and F. Bechstedt, Quasiparticle band structures of the antiferromagnetic transition-metal oxides MnO, FeO, CoO, and NiO, Phys. Rev. B **79**, 235114 (2009).

[20] B. Cunningham, M. Grüning, D. Pashov, and M. Van Schilfgaarde, QS$G\widehat{W}$: Quasiparticle self-consistent *GW* with ladder diagrams in W, Phys. Rev. B **108**, 165104 (2023).

[21] J. M. Tomczak, M. Casula, T. Miyake, and S. Biermann, Asymmetry in band widening and quasiparticle lifetimes in $SrVO_3$: Competition between screened exchange and local correlations from combined *GW* and dynamical mean-field theory *GW* + DMFT, Phys. Rev. B **90**, 165138 (2014).

[22] L. Boehnke, F. Nilsson, F. Aryasetiawan, and P. Werner, When strong correlations become weak: Consistent merging of *GW* and DMFT, Phys. Rev. B **94**, 201106 (2016).

[23] K. Held, I. A. Nekrasov, G. Keller, V. Eyert, N. Blümer, A. K. McMahan, R. T. Scalettar, T. Pruschke, V. I. Anisimov, and D. Vollhardt, Realistic investigations of correlated electron systems with LDA + DMFT, Phys. Status Solidi B **243**, 2599 (2006).

[24] G. Kotliar, S. Y. Savrasov, K. Haule, V. S. Oudovenko, O. Parcollet, and C. A. Marianetti, Electronic structure calculations with dynamical mean-field theory, Rev. Mod. Phys. **78**, 865 (2006).

[25] A. Paul and T. Birol, Applications of DFT + DMFT in materials science, Annu. Rev. Mater. Res. **49**, 31 (2019).

[26] P. W. Anderson, Localized magnetic states in metals, Phys. Rev. **124**, 41 (1961).

[27] E. Gull, A. J. Millis, A. I. Lichtenstein, A. N. Rubtsov, M. Troyer, and P. Werner, Continuous-time Monte Carlo methods for quantum impurity models, Rev. Mod. Phys. **83**, 349 (2011).

[28] P. Werner, Dynamical mean-field theory of correlated electrons, Forschungszentrum Jülich **12** (2022).

[29] S. Iskakov, C.-N. Yeh, E. Gull, and D. Zgid, *Ab initio* self-energy embedding for the photoemission spectra of NiO and MnO, Phys. Rev. B **102**, 085105 (2020).

[30] T. Zhu and G. K.-L. Chan, *Ab initio* full cell *GW* + DMFT for correlated materials, Phys. Rev. X **11**, 021006 (2021).

[31] J. van Elp, J. L. Wieland, H. Eskes, P. Kuiper, G. A. Sawatzky, F. M. F. de Groot, and T. S. Turner, Electronic structure of CoO, Li-doped CoO, and $LiCoO_2$, Phys. Rev. B **44**, 6090 (1991).

[32] T. Chiarotti, A. Ferretti, and N. Marzari, Energies and spectra of solids from the algorithmic inversion of dynamical Hubbard functionals, Phys. Rev. Res. **6**, L032023 (2024).

[33] S. Backes, T. C. Rödel, F. Fortuna, E. Frantzeskakis, P. Le Fèvre, F. Bertran, M. Kobayashi, R. Yukawa, T. Mitsuhashi, M. Kitamura, *et al.*, Hubbard band versus oxygen vacancy states in the correlated electron metal $SrVO_3$, Phys. Rev. B **94**, 241110 (2016).

[34] F. Petocchi, F. Nilsson, F. Aryasetiawan, and P. Werner, Screening from e_g states and antiferromagnetic correlations in $d^{(1,2,3)}$ perovskites: A *GW* + EDMFT investigation, Phys. Rev. Res. **2**, 013191 (2020).

[35] The double-counting correction of the dynH functional is defined in Eq. (7) of Ref. [32]. The constant c allows to fix the gauge of the static double counting term. In the present calculations, this static term is taken to be the averaged local matrix elements of the bare screened interaction, i.e., the high-frequency limit $U(\omega \to \infty \equiv U^{\infty})$.

[36] The spin dependence of the local basis is related to spin dependence of the Wannier functions used as projectors in the $U(\omega)$ calculation, to the orthoatomic projectors used in Eq. (1), which bear no spin dependency. The MLWF [49] was built from the TM $3d$, $3p$, $4s$, and O $2p$ orbitals.

[37] D. Golze, M. Dvorak, and P. Rinke, The *GW* compendium: A practical guide to theoretical photoemission spectroscopy, Front. Chem. **7**, 377 (2019) .

[38] S. Höfner, P. Steiner, I. Sander, F. Reinert, and H. Schmitt, The optical gap of NiO, Z. Phys. B **86**, 207 (1992).

[39] S. L. Dudarev, G. A. Botton, S. Y. Savrasov, C. J. Humphreys, and A. P. Sutton, Electron-energy-loss spectra and the structural stability of nickel oxide: An LSDA+U study, Phys. Rev. B **57**, 1505 (1998).

[40] M. Vanzini and N. Marzari, Towards a minimal description of dynamical correlation in metals, arXiv:2309.12144.

[41] T. Chiarotti, N. Marzari, and A. Ferretti, Unified Green's function approach for spectral and thermodynamic properties from algorithmic inversion of dynamical potentials, Phys. Rev. Res. **4**, 013242 (2022).

[42] R. N. Silver, D. S. Sivia, and J. E. Gubernatis, Maximum-entropy method for analytic continuation of quantum Monte Carlo data, Phys. Rev. B **41**, 2380 (1990).

[43] See Supplemental Material at https://link.aps.org/supplemental/10.1103/y7gb-q22g for the DFT electronic structure obtained with r2SCAN, the sum-over-poles representation of the local screened Coulomb interaction $U(\omega)$, the role of dynamical screening and a comparison with static DFT+U, the DFT+dynH projected densities of states, and full computational details, which includes Refs. [44,50–61].

[44] J. W. Furness, A. D. Kaplan, J. Ning, J. P. Perdew, and J. Sun, Accurate and numerically efficient r^2 SCAN meta-generalized gradient approximation, J. Phys. Chem. Lett. **11**, 8208 (2020).

[45] In passing, we note that with LDA/PBEsol functionals, owing to their wrong metallic solutions for FeO and CoO, the effective screened interactions for the two compounds are overscreened. The choice to use r2SCAN as the DFT starting point has then the advantage of properly capture the insulating nature of the ground states for all four compounds, thus allowing for a better quantitative prediction of gap magnitudes.

[46] J. Bała, A. M. Oleś, and J. Zaanen, Zhang-Rice localization, quasiparticle dispersions, and the photoemission of NiO, Phys. Rev. Lett. **72**, 2600 (1994).

[47] F. C. Zhang and T. M. Rice, Effective Hamiltonian for the superconducting Cu oxides, Phys. Rev. B **37**, 3759 (1988).

[48] Note that this is consistent with the high-spin 5/2 configuration of the d^5 shell in Mn^{2+} being more mean-field-like.

[49] N. Marzari, A. A. Mostofi, J. R. Yates, I. Souza, and D. Vanderbilt, Maximally localized Wannier functions: Theory and applications, Rev. Mod. Phys. **84**, 1419 (2012).

[50] P. Giannozzi, S. Baroni, N. Bonini, M. Calandra, R. Car, C. Cavazzoni, D. Ceresoli, G. L. Chiarotti, M. Cococcioni, I. Dabo, *et al.*, QUANTUM ESPRESSO: A modular and open-source software project for quantum simulations of materials, J. Phys.: Condens. Matter **21**, 395502 (2009).

[51] D. R. Hamann, Optimized norm-conserving Vanderbilt pseudopotentials, Phys. Rev. B **88**, 085117 (2013).

[52] M. J. van Setten, M. Giantomassi, E. Bousquet, M. J. Verstraete, D. R. Hamann, X. Gonze, and G. M. Rignanese, The PseudoDojo: Training and grading a 85 element optimized norm-conserving pseudopotential table, Comput. Phys. Commun. **226**, 39 (2018).

[53] K. Nakamura, Y. Yoshimoto, Y. Nomura, T. Tadano, M. Kawamura, T. Kosugi, K. Yoshimi, T. Misawa, and Y. Motoyama, RESPACK: An *ab initio* tool for derivation of effective low-energy model of material, Comput. Phys. Commun. **261**, 107781 (2021).

[54] T. Chiarotti, Spectral and thermodynamic properties of interacting electrons with dynamical functionals, Ph.D. thesis, EPFL, Lausanne, Switzerland, 2023.

[55] H. Fjellvåg, F. Grønvold, S. Stølen, and B. Hauback, On the crystallographic and magnetic structures of nearly stoichiometric iron monoxide, J. Solid State Chem. **124**, 52 (1996).

[56] A. Cheetham and D. Hope, Magnetic ordering and exchange effects in the antiferromagnetic solid solutions $Mn_xNi_{1-x}O$, Phys. Rev. B **27**, 6964 (1983).

[57] W. Johnston and R. Heikes, A study of the $Li_xMn_{(1-x)}O$ system, J. Am. Chem. Soc. **78**, 3255 (1956).

[58] C. McCammon and L.-G. Liu, The effects of pressure and temperature on nonstoichiometric wöstite, FexO: The iron-rich phase boundary, Phys Chem Minerals **10**, 106 (1984).

[59] M. Carey, F. Spada, A. Berkowitz, W. Cao, and G. Thomas, Preparation and structural characterization of sputtered CoO, NiO, and $Ni_{0.5}Co_{0.5}O$ thin epitaxial films, J. Mater. Res. **6**, 2680 (1991).

[60] L. Bartel and B. Morosin, Exchange striction in NiO, Phys. Rev. B **3**, 1039 (1971).

[61] D. Herrmann-Ronzaud, P. Burlet, and J. Rossat-Mignod, Equivalent type-II magnetic structures: CoO, a collinear antiferromagnet, J. Phys. C: Solid State Phys. **11**, 2123 (1978).